Proc. of the European Safety and Reliability Conference (ESREL 2026)
Edited by José C. Matos, Paulo B. Lourenço, Michael Beer, Daniel Oliveira,
Edoardo Patelli, Hélder S. Sousa, Rui A. Silva and Monica Santamaria
 Published by Research Publishing, Singapore.
doi: 10.3850/ESREL2026061419_esrel26-p27813-cd

Localized Reduced-Order Modeling via Parameter Space Splitting for the Prediction of Contaminant Dispersion in Urban Areas

Lisa Kühn[1,*], Jacopo Bonari[1], Max von Danwitz[1], Alexander Popp[1,2]

[1] *German Aerospace Center (DLR), Institute for the Protection of Terrestrial Infrastructures, Germany.*

[2] *University of the Bundeswehr Munich, Institute for Mathematics and Computer-Based Simulation, Germany.*

[*] *Corresponding author. E-mail: lisa.kuehn@dlr.de*

Numerical simulations of accidental contaminant releases, such as gas leaks at chemical plants, can provide meaningful information about the dispersion of hazardous substances during emergency response actions and in preparatory studies involving many different ”what-if” scenarios. Common models couple the incompressible Navier–Stokes equations for the assessment of the wind field with an advection–diffusion problem for evaluating the contaminant transport from an instantaneous source. However, computational times required to evaluate such high-fidelity models grow substantially with increasing model complexity. This limits their feasibility for time-critical applications, and motivates the use of model-order reduction techniques for rapid yet reliable online predictions based on prior offline computations. Therefore, a non-intrusive, purely data-driven reduced-order model (ROM) is developed that accounts for different wind conditions. The ROM is built for a two-dimensional domain that reproduces realistic building footprints, preserving key features necessary for studying the dispersion across developed areas. Due to the complexity of the problem, a global ROM covering the complete parameter space provides insufficient approximations. Thus, a localized approach is employed, setting up and aggregating local reduced-order models each corresponding to a sub-range of a split-up parameter space. Ultimately, the developed model approximates the spatio-temporal concentration field for a certain time frame with a mean relative error below 3%, while providing predictions around 100 times faster than the original full-order high-fidelity model.

Keywords: airborne contaminant transport, crisis management, reduced-order modeling, proper orthogonal decomposition with interpolation, parameter space splitting.

1. Introduction

Chemical incidents pose significant risks to public safety and infrastructures with many reported incidents over the years. Computational modeling of contaminant dispersion can support both preparatory analysis and emergency response. While Gaussian plume models (Snoun et al., 2023) are widely used for their computational efficiency, they rely, in their basic form, on simplifying assumptions such as continuous point-source emissions and downwind dispersion following a normal distribution. These idealizations limit their reliability in urban environments, where buildings and complex topographies significantly alter flows and dispersion patterns. To address these shortcomings, high-fidelity computational fluid dynamics (CFD) models solve steady-state incompressible Navier-Stokes (INS) equations for more realistic wind field predictions and couple them with an advection-diffusion (AD) problem to simulate contaminant transport (Hinsen et al., 2023). Although these models can offer superior accuracy, their high computational cost quickly restrict their use for time-critical applications such as emergency response or multi-query risk assessments for complex geometries. Model order reduction (MOR) can provide a promising way to enable fast and accurate predictions by deriving a reduced-order model (ROM) that approximates the full-order model (FOM), such as the aforementioned CFD-based dispersion process, with much lower computational cost than the FOM. To this end, the process is separated into two phases: (i) an offline phase, where high-fidelity FOM simulations are computed, based on which the ROM is set up, and (ii) an online phase, where the ROM is evaluated independently of the FOM. Two main strategies exist: (i) intrusive methods, e.g., proper orthogonal decomposition

(POD) followed by a Galerkin projection of the FOM operators (PODG) (Quarteroni et al., 2015), and (ii) non-intrusive methods such as POD with interpolation (PODI) (Bui-Thanh et al., 2003) or other purely data-driven machine-learning based methods. Whereas the first approach exploits the underlying physics of the system, yet requiring access to FOM operators, non-intrusive methods solely rely on FOM data, thus avoiding solver dependencies. Non-intrusive ROMs are thereby particularly attractive in some cases, as they commonly provide large speed-ups, bypass the need for explicit hyper-reduction and are compatible with legacy or proprietary solvers. However, they often require large training data sets and, depending on the used method, can suffer from overfitting or sensitivity to hyper-parameters (Czech et al., 2022). Moreover, POD-based methods approximate the FOM solution space with a linear subspace making it difficult to approximate nonlinear solutions on a low-dimensional subspace. Such problems can be identified by a slow decay of the Kolmogorov n-width, as is the case for highly advection-dominated problems (Quarteroni et al., 2015). To overcome this, techniques such as autoencoders (Maulik et al., 2021), operator learning (Melchers et al., 2026), nonlinear manifold methods (Schwerdtner and Peherstorfer, 2024), or piecewise linear subpaces (Amsallem et al., 2012), as applied here, are increasingly employed.

ROMs for gas dispersion simulations across urban areas have already proven effective for diverse applications, especially with focus on air pollution modeling (Khamlich et al., 2023). Furthermore, ROMs have been investigated for wind fields in urban settings, e.g., for drone routing (Veiga-Piñeiro et al., 2024). Additionally, multiple studies were conducted introducing ROMs of the AD problem for simple benchmark geometries, some also under varying wind conditions as in Melchers et al. (2026), and publications computing a ROM for the AD problem with a fixed wind field (Ritter et al., 2016; Mattuschka et al., 2026). For a varying wind field, a hybrid ROM combining PODG and PODI was recently applied to the coupled problem for air pollution prediction in Khamlich et al. (2023). Yet, ROMs for chemical accidents under varying wind conditions remain scarcely studied. Based on a previous study in (Kühn et al., 2026), this work therefore introduces a non-intrusive ROM based on localized PODI to predict the spatio-temporal evolution of contaminant concentration in built-up areas under changing wind direction and velocity. By its non-intrusive nature, the ROM avoids explicit hyper-reduction schemes for nonlinear and non-affine terms as needed for projection-based intrusive methods, as well as it circumvents tuning hyper-parameters of NN-based approaches. To further minimize the number of parameters, time is treated as an additional dimension rather than a separate parameter (Bērziņš et al., 2020). The framework is employed on a two-dimensional laminar flow over a geometrically realistic domain derived from open-access building footprints, capturing key dispersion features corresponding to neutrally buoyant or gases denser than air. Despite the two-dimensional simplification, the setup preserves essential physical behavior and serves as a foundation for future extensions to three-dimensional geometries and state-of-the-art turbulence modeling. The paper is structured as follows: Section 2 outlines the governing equations for the FOM, whereas Section 3 recapitulates PODI. Section 4 follows by presenting the ROM and its performance on the chosen numerical example. The article is concluded in Section 5.

2. Full-Order Model

To model the transport of airborne contaminants in a two-dimensional bounded domain $\Omega \subseteq \mathbb{R}^2$, the flow field is obtained in a first step by solving the steady-state INS equations and subsequently addressing the contaminant dynamics by means of an AD problem. The INS equations for the velocity vector field $\mathbf{u}$ and pressure p, parametrized for different inflow wind velocities and directions, are given by:

$$\begin{aligned}
-\nu\nabla^2\mathbf{u} + (\mathbf{u}\cdot\nabla)\mathbf{u} + \nabla p &= \mathbf{0} && \text{in} \quad \Omega,\\
\nabla\cdot\mathbf{u} &= 0 && \text{in} \quad \Omega,\\
\mathbf{u} &= \mathbf{g}_D(\boldsymbol{\mu}) && \text{on} \quad \Gamma_D,\\
\mathbf{u} &= \mathbf{0} && \text{on} \quad \Gamma_0.
\end{aligned} \tag{1}$$

Herein, $\nu \in \mathbb{R}^+$ denotes the kinematic viscosity, Γ_0 the boundaries at the buildings, and the parameters $\boldsymbol{\mu} \in \mathcal{D} \subset (\mathbb{R}^+ \times [0, 2\pi])$ account for variable inflow wind conditions via the Dirichlet boundary condition. The latter is described as $\mathbf{g}_\mathrm{D} = w_\mathrm{i}[\cos(w_\mathrm{d}), \sin(w_\mathrm{d})]^\intercal$, parametrized by the respective values for the inflow wind velocity $w_\mathrm{i} \in \mathbb{R}^+$ in $\mathrm{m\,s^{-1}}$ and the direction $w_\mathrm{d} \in [0, 2\pi]$. This yields an enclosed INS problem without a Neumann boundary condition, corresponding to the formulation discussed in (Elman et al., 2014, Sec. 9.3.5). Consequently, the velocity $\mathbf{u}$ and pressure p are parametrized quantities $(\mathbf{u}, p) = \big(\mathbf{u}(\mathbf{x}, \boldsymbol{\mu}), p(\mathbf{x}, \boldsymbol{\mu})\big)$. Eventually, the Reynolds number is computed from the peak velocity $u_{\max}$, the characteristic size of the cumulated building imprints l which is represented by the diameter of the region of refined mesh around the buildings in Fig. 1, and the viscosity ν.

To obtain a numerical solution for the flow velocity field, Eq.(1) is first reformulated into its weak form and then discretized using a Taylor-Hood finite element scheme. The resulting nonlinear system of equations is solved iteratively via the Newton-Raphson method, as implemented in the open-source finite element toolbox FEniCS (Alnaes et al., 2015). Upon deriving the wind field $\mathbf{u}(\mathbf{x}, \boldsymbol{\mu})$, the AD problem

$$
\begin{aligned}
\frac{\partial c}{\partial t} - \kappa \nabla^2 c + \mathbf{u} \cdot \nabla c = 0 \quad & \text{in } \Omega \times (0, T)\,, \\
\kappa \nabla c \cdot \mathbf{n} = 0 \quad & \text{in } (\Gamma_+ \cup \Gamma_0) \times (0, T)\,, \\
c(\mathbf{x}, t) = 0 \quad & \text{in } \Gamma_- \times (0, T)\,, \\
c(\mathbf{x}, 0) = m(\mathbf{x}) \quad & \text{in } \Omega,
\end{aligned}
\tag{2}
$$

can be solved for the spatio-temporal gas concentration $c(\mathbf{x}, t; \boldsymbol{\mu}) \in \mathbb{R}^+$. The model is governed by the diffusion coefficient $\kappa \in \mathbb{R}^+$, while, following Elman et al. (2014), $\Gamma_+ \subset \partial\Omega$ denotes the outflow boundary with $\mathbf{u} \cdot \mathbf{n} > 0$, $\Gamma_0 \subset \partial\Omega$ the boundaries tangential to the flow such that $\mathbf{u} \cdot \mathbf{n} = 0$ and $\Gamma_- \subset \partial\Omega$ the inflow boundary with $\mathbf{u} \cdot \mathbf{n} < 0$. For the numerical solution of the AD problem, a first-order Lagrange finite element approach is selected with a SUPG-stabilized weak form for the boundary value problem (von Danwitz et al., 2023), and an implicit backward Euler time-stepping algorithm (Elman et al., 2014), Eq. (10.25). This yields the concentration field $\mathbf{c}(t; \boldsymbol{\mu}) \in \mathbb{R}^{N_\mathrm{h}}$ with N_h denoting the degrees of freedom of the FEM model.

3. Reduced-Order Model

The ROM is set up via POD to find a reduced basis (RB), followed by an interpolation to map unseen parameter values to a respective approximate solution of Eq. (2). For a more extensive description of the method, the interested reader is pointed towards (Kühn et al., 2026).

3.1. *Proper orthogonal decomposition*

To create a RB, POD relies on snapshot solutions of Eq. (2) for an a-priori chosen set of training parameter values $\Xi_\mathrm{s} = \{\boldsymbol{\mu}_1, \ldots, \boldsymbol{\mu}_{N_\mathrm{s}}\}$. These N_s snapshots are collected within the snapshot matrix $\mathbf{S} = [\mathbf{c}_1, \ldots, \mathbf{c}_{N_\mathrm{s}}] \in \mathbb{R}^{N_\mathrm{h,st} \times N_\mathrm{s}}$. Hereby, each snapshot solution $\mathbf{c}_k \in \mathbb{R}^{N_\mathrm{h,st}}$ represents the FOM concentration field in space-time format for the k^th parameter value pair $(w_\mathrm{d}^k, w_\mathrm{i}^k)$ in Ξ_s:

$$
\mathbf{c}_k = [\mathbf{c}(t_1; \boldsymbol{\mu}_k)^\intercal, \ldots, \mathbf{c}(t_e; \boldsymbol{\mu}_k)^\intercal]^\intercal. \tag{3}
$$

Based on these snapshots, POD identifies the low-dimensional subspace $\mathcal{V} = \mathrm{span}\{\mathbf{V}\}$, generated by the column-orthogonal basis matrix $\mathbf{V} = [\mathbf{V}_1, \ldots, \mathbf{V}_{N_\mathrm{rb}}] \in \mathbb{R}^{N_\mathrm{h,st} \times N_\mathrm{rb}}$. For this purpose, a singular value decomposition of the snapshot matrix $\mathbf{S} = \mathbf{U}\boldsymbol{\Sigma}\mathbf{Z}^\intercal$ can be performed. The RB vectors can then be derived from the orthogonal matrix $\mathbf{U} = [\boldsymbol{\Phi}_1, \ldots, \boldsymbol{\Phi}_{N_\mathrm{h,st}}] \in \mathbb{R}^{N_\mathrm{h,st} \times N_\mathrm{h,st}}$ by selecting the modes $\boldsymbol{\Phi}_i$ that correspond to the largest $N_\mathrm{rb} \ll N_\mathrm{h,st}$ eigenvalues σ_i in $\boldsymbol{\Sigma} = \mathrm{diag}\,(\sigma_1, \ldots, \sigma_r) \in \mathbb{R}^{N_\mathrm{h,st} \times N_\mathrm{s}}$, where $\sigma_1 \geq \ldots \geq \sigma_r$, and $r \leq \min(N_\mathrm{h,st}, N_\mathrm{s})$ denotes the rank of $\mathbf{S}$ (Quarteroni et al., 2015). With the basis matrix $\mathbf{V} = [\boldsymbol{\Phi}_1, \ldots, \boldsymbol{\Phi}_{N_\mathrm{rb}}] \in \mathbb{R}^{N_\mathrm{h,st} \times N_\mathrm{rb}}$, the concentration in space-time format can be approximated by a linear combination of parameter-independent POD modes and parameter-dependent POD coefficients:

$$
\mathbf{c}(\boldsymbol{\mu}) \approx \sum_{i=1}^{N_\mathrm{rb}} a_i(\boldsymbol{\mu}) \boldsymbol{\Phi}_i = \mathbf{V}\mathbf{a}(\boldsymbol{\mu}). \tag{4}
$$

Ultimately, a direct relationship between the POD error and the neglected eigenvalues can be derived, highlighting the importance of rapidly decaying eigenvalues. Accordingly, the energy retained by the ROM can be expressed as:

$$E_{\mathrm{rb}} = \frac{\sum_{i=1}^{N_{\mathrm{rb}}} \sigma_i}{\sum_{k=1}^{r} \sigma_k} \quad \in [0, 1]. \tag{5}$$

3.2. *POD with interpolation*

Based on the reduced basis, PODI (Bui-Thanh et al., 2003) approximates the FOM solution for unseen parameter values by evaluating an interpolation scheme for the POD coefficients. Since PODI is a non-intrusive method, it relies only on the snapshot data and, in a first step, projects them onto the linear subspace. This derives an approximation of the snapshot data as shown in Eq. (4) and with it a set of known coefficients $a_i(\boldsymbol{\mu}_k) = (\boldsymbol{\Phi}_i, \mathbf{c}(\boldsymbol{\mu}_k))_{L^2} \in \mathbb{R}$, $k = 1, \ldots, N_{\mathrm{s}}$, to set up an interpolation scheme to approximate the mapping of parameter values to POD coefficients $\boldsymbol{\pi} : \mathcal{D} \rightarrow \mathbb{R}^{N_{\mathrm{rb}}}$, $a_i(\boldsymbol{\mu}) \approx \boldsymbol{\pi}_i(\boldsymbol{\mu})$. For that purpose, a thin-plate spline radial basis function $\varphi(d) = d^2 \log(d)$ is used:

$$\boldsymbol{\pi}(\boldsymbol{\mu}) = \sum_{k=1}^{N_{\mathrm{s}}} \mathbf{w}_k \varphi(\|\boldsymbol{\mu} - \boldsymbol{\mu}_k\|), \tag{6}$$

where $\pi_i(\boldsymbol{\mu}_k) = a_i(\boldsymbol{\mu}_k)$, $i = 1, \ldots, N_{\mathrm{rb}}$ and d is the Euclidean distance between a sample point $\boldsymbol{\mu}$ and the parameter value pair $\boldsymbol{\mu}_k$ evaluated when computing the snapshots. Although the lack of physical relations holds its drawbacks, PODI allows for a flexible and straightforward application that avoids hyper-reduction for the Dirichlet boundary condition as well as the convective term, and is applicable for closed-source solvers not granting access to FOM operators. The implementation presented in this work is based on the open-source toolbox EZyRB (Demo et al., 2018).

3.3. *Parameter space splitting*

To achieve significantly accelerated evaluations via the ROM, a low-dimensional RB is essential. However, as mentioned in Sec. 1, this cannot be guaranteed for advection-dominated problems as considered here. To facilitate the setup of ROMs with a small RB, the parameter space can be split and efficient local ROMs can be set up for the respective sub-ranges (Bhat et al., 2025). Eventually, during the online phase, the respective local ROM is chosen for the final evaluation by assessing the given parameter value.

4. Numerical Example

4.1. *Setup*

The computational domain, representing an excerpt of a chemical site located in Düsseldorf, Germany, is derived as described in Bonari et al. (2024) and shown in Fig. 1 with its computational mesh. Further details of the setup are provided in Tab. 1, while Fig. 2a illustrates the parameter space splitting. As shown in Fig. 2b, snapshots of the coupled problem are collected at (i) equidistantly sampled wind directions and velocities $w_{\mathrm{i}} \geq 1.8\,\mathrm{m\,s^{-1}}$, and (ii) logarithmic samples for lower velocities. Each snapshot spans 50 time steps, resulting in a space-time solution vector as defined in Eq. (3). The complexity of the time-dependent, nonlinear coupled problem is evident from the slow decay of the normalized eigenvalues and the retained energy curves for different RB sizes, shown in Fig. 3. To avoid requiring an extensive number of RB functions, eight local ROMs are introduced, each trained for a $45°$ sub-range of the inflow wind direction, thereby dividing the full range into eight equal intervals, Fig. 2a. The number of training snapshots per local ROM is accordingly reduced to 23×45 as specified in Tab. 1. By significantly reducing the complexity each local ROM has to capture, the eigenvalues of the correlation matrix in Fig. 3 decay much faster, indicating that a smaller RB may be sufficient. To evaluate the ROM performance, additional FOM snapshots are generated at the same time steps as before, but with wind velocities midway between training values and wind directions coinciding with training values. The rationale for the latter lies in the assumption that, given typical sensor accuracies, evaluations between already densely sampled wind directions are of limited practical interest. Nevertheless, the ROM remains functional for such cases, though higher errors may occur than those reported here.

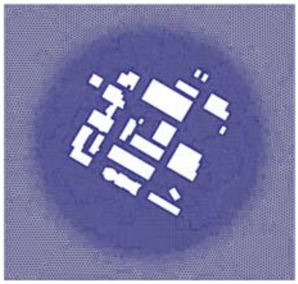

Fig. 1.: The considered geometry, additionally featuring the employed mesh discretization.

Table 1.: Parameters of the full-order and reduced-order model featuring a parametric dependence on the inflow wind velocity and direction.

Parameter	**Value**
Domain size (m)	750×717
Time (s)	$t \in [0, 1, \ldots, 50]$
Degrees of freedom	21,616
Reynolds number	$Re \in [4, 180]$
Inflow wind velocity $(\mathrm{m\,s^{-1}})$	$w_{\mathrm{i}} \in [0.3, 10]$
Inflow wind direction (deg)	$w_{\mathrm{d}} \in [0, 360]$
Training set samples (global | local) w_{i}	23 | 23
Training set samples (global | local) w_{d}	360 | 45
Test set samples (global | local) w_{i}	8 | 8
Test set samples (global | local) w_{d}	72 | 9

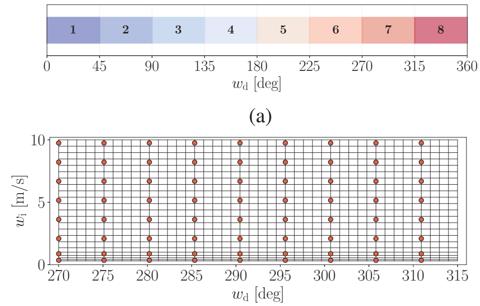

(b)

Fig. 2.: Visualization of the split up parameter space (a) and sampling points for training and testing of the ROM corresponding to the 7$^{\mathrm{th}}$ subrange (b). Intersections of the grid lines mark the training parameter values, circles indicate testing parameter values.

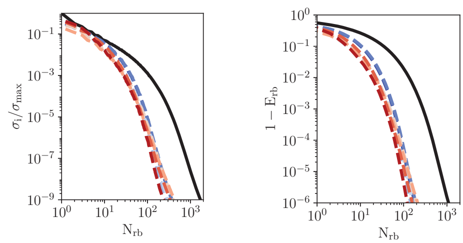

(b)

Fig. 3.: Normalized eigenvalues of the snapshot correlation matrix (a), and retained energy (b) as a function of the reduced basis size. The colorful dashed lines represent data for the local ROMs, while the black bold line represents the global ROM.

4.2. *Results*

Evaluating the L^2-error for varying sizes of the RB in Fig. 4a confirms what was indicated by the rapid decay of the eigenvalues of Fig. 3a. Compared to the global ROM, the mean relative L^2-error of the local ROMs decreases significantly faster as the RB size increases, achieving substantially lower errors for the same RB dimension. The relative L^2-error is hereby computed across the domain, while the mean averages the errors for the different test parameter values. A second important quantity is the speed-up shown in Fig. 4b. Here, it can be observed that the speed-up of local and global ROMs decreases with the size of the RB, enabling an evaluation which is around 100 times faster than the FOM. However, keeping in mind the improved approximation quality of the localized ROMs, they are preferable for the presented case. An impression of the spatial contraction field obtained by FOM and ROM can be seen in Fig. 5.

5. Conclusion and Outlook

In this paper, a ROM has been presented to accelerate accurate dispersion predictions of airborne contaminants that originate from a known, instantaneous source and get transported across a built-up area according to current wind conditions. The study focuses on a two-dimensional cross-section of a chemical plant, incorporating

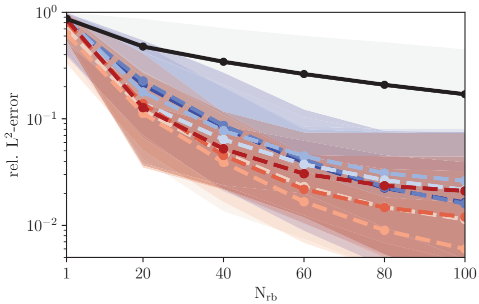

(a)

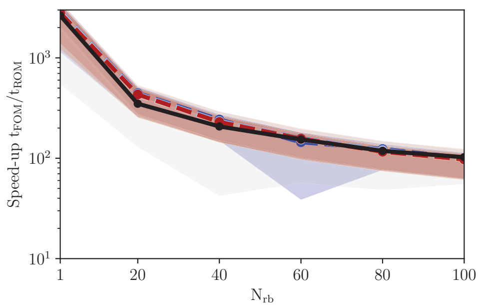

(b)

Fig. 4.: Relative L^2-error (a) and speed-up (b) for varying RB sizes. Results of the global ROM are shown in black, while local ROMs are represented as colorful dashed lines. The mean values are indicated by bold lines, while shaded areas indicate the range between minimum and maximum error or speed-up for the different test parameter values.

local building layouts. An aggregated ROM has been introduced consisting of eight local ROMs, each set up for a specific sub-range of the wind direction. The temporal aspect of the transient problem has been handled via a space-time data format, thus reducing the number of parameters during the reduction. Although not required here, the approach preserves the possibility of evaluating the solution between precomputed time steps via linear interpolation. Besides circumventing the need for a dedicated approximation scheme for nonlinear and non-affine terms, the proposed non-intrusive ROM is set up without accessing the FOM operators. The latter also allows for flexible application to other scenarios like flooding as considered in (Schneider et al., 2026). The use of local ROMs results in approximation errors below 3% while providing a speed-up of approximately 100. Compared to a look-up table of precomputed results, which requires less computational effort, but for that only allows qualitative estimates for wind velocities not included in the table, the proposed ROM enables quantitative predictions across continuous parameter variations for the wind velocity, offering greater flexibility and accuracy. Due to the chosen approach, the temporal prediction is limited to the predefined time span, making it unfeasible for temporal extrapolation. It is also reminded that the errors shown above are valid for evaluating wind directions covered during the ROM setup only, assuming that no evaluation is needed in-between. Lastly, the approach poses some requirements on the available memory to load all eight local ROMs in parallel as it might be needed during the online evaluation. This can be troublesome, if larger RBs need to be chosen for the local ROMs and light devices are being used during the online phase. Because of these points and to further increase the speed-up, nonlinear methods that are able to provide accurate predictions on smaller latent spaces as well as accounting for temporal extrapolation are research directions to be further investigated. Future work will furthermore extend the ROM to three-dimensional domains and apply it to source-identification (Mattuschka et al., 2026). Moreover, to support crisis management and preparatory analysis, future studies will aim to make simulation results easily accessible and well-integrated into decision-supporting systems as in (Schneider et al., 2025).

Acknowledgments

A.P. acknowledges support by *dtec.bw - Digitalization and Technology Research Center of the Bundeswehr* (project *RISK.twin*). dtec.bw is funded by the European Union - NextGenerationEU. The authors gratefully acknowledge the computational and data resources provided through the joint high-performance data analytics (HPDA) project "terrabyte" of the German Aerospace Center (DLR) and the Leibniz Supercomputing Center (LRZ).

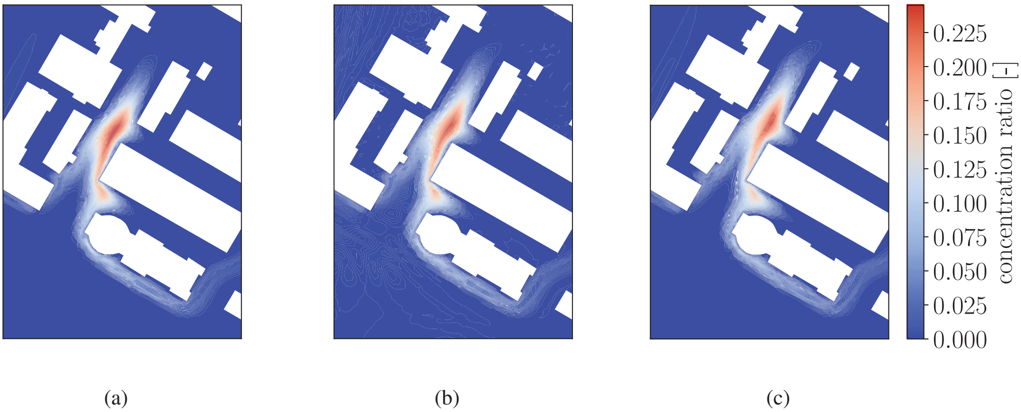

Fig. 5.: Concentration fields at $t = 50\,\mathrm{s}$. FOM result at $w_\mathrm{d} = 45°$, $w_\mathrm{i} = 9.49\,\mathrm{m\,s^{-1}}$ (a), ROM prediction at $w_\mathrm{d} = 45°$, $w_\mathrm{i} = 9.74\,\mathrm{m\,s^{-1}}$ (b), and FOM result at $w_\mathrm{d} = 45°$, $w_\mathrm{i} = 10.0\,\mathrm{m\,s^{-1}}$ (c).

References

Alnaes, M. S., J. Blechta, J. Hake, A. Johansson, B. Kehlet, A. Logg, C. N. Richardson, J. Ring, M. E. Rognes, and G. N. Wells (2015). The FEniCS project version 1.5. *Archive of Numerical Software 3*. 10.11588/ans.2015.100.20553.

Amsallem, D., M. J. Zahr, and C. Farhat (2012). Nonlinear model order reduction based on local reduced–order bases. *International Journal for Numerical Methods in Engineering 92*(10), 891–916. 10.1002/nme.4371.

Bhat, S. P., N. Barral, and M. Ricchiuto (2025). Error-based efficient parameter space partitioning for mesh adaptation and local reduced order models. *Computer Methods in Applied Mechanics and Engineering 435*, 117649. 10.1016/j.cma.2024.117649.

Bonari, J., L. Kühn, M. v. Danwitz, and A. Popp (2024). Towards real-time urban physics simulations with digital twins. In *2024 28th International Symposium on Distributed Simulation and Real Time Applications (DS-RT)*, pp. 18–25. IEEE. 10.1109/DS-RT62209.2024.00013.

Bui-Thanh, T., M. Damodaran, and K. Willcox (2003). Proper orthogonal decomposition extensions for parametric applications in compressible aerodynamics. In *21st AIAA Applied Aerodynamics Conference*, Reston, Viriginia. American Institute of Aeronautics and Astronautics. 10.2514/6.2003-4213.

Bērziņš, A., J. Helmig, F. Key, and S. Elgeti (2020). Standardized non-intrusive reduced order modeling using different regression models with application to complex flow problems. 10.48550/arXiv.2006.13706.

Czech, C., M. Lesjak, C. Bach, and F. Duddeck (2022). Data-driven models for crashworthiness optimisation: intrusive and non-intrusive model order reduction techniques. *Structural and Multidisciplinary Optimization 65*(7), 190. 10.1007/s00158-022-03282-1.

Demo, N., M. Tezzele, and G. Rozza (2018). EZyRB: Easy Reduced Basis method. *The Journal of Open Source Software 3*(24), 661. 10.21105/joss.00661.

Elman, H. C., D. J. Silvester, and A. J. Wathen (2014). *Finite elements and fast iterative solvers: with applications in incompressible fluid dynamics* (Second ed.). Numerical mathematics and scientific computation. Oxford: Oxford University Press.

Hinsen, P., T. Wiedemann, D. Shutin, and A. J. Lilienthal (2023). Exploration and gas source localization in advection–diffusion processes with potential-field-controlled robotic swarms. *Sensors 23*(22). 10.3390/s23229232.

Khamlich, M., G. Stabile, G. Rozza, L. Környei, and Z. Horváth (2023). A physics-based reduced order model for urban air pollution prediction. *Computer Methods in Applied Mechanics and Engineering 417*, 116416. 10.1016/j.cma.2023.116416.

Kühn, L., J. Bonari, M. v. Danwitz, and A. Popp (2026). Intrusive and non-intrusive model order reduction for airborne contaminant transport: Comparative analysis and uncertainty quantification. 10.48550/arXiv.2602.21996.

Mattuschka, M., N. An der Lan, M. von Danwitz, D. Wolff, and P. Alexander (2026). Goal-oriented optimal sensor placement for pde-constrained inverse problems in crisis management. *Computer Assisted Methods in Engineering and Science*. 10.24423/cames.2026.1887.

Mattuschka, M., J. Bonari, M. v. Danwitz, and A. Popp (2026). Rapid identification of moving contaminant sources through physics-based modelling. 10.48550/arXiv.2603.12969.

Maulik, R., B. Lusch, and P. Balaprakash (2021). Reduced-order modeling of advection-dominated systems with recurrent neural networks and convolutional autoencoders. *Physics of Fluids 33*(3), 037106. 10.1063/5.0039986.

Melchers, H. A., J. Prins, and M. Abdelmalik (2026). Neural green's operators for parametric partial differential equations. *Computer Methods in Applied Mechanics and Engineering 455*, 118893. 10.1016/j.cma.2026.118893.

Quarteroni, A., A. Manzoni, and F. Negri (2015). *Reduced basis methods for partial differential equations: An introduction*, Volume 92 of *UNITEXT La Matematica per il 3+2*. Cham: Springer. 10.1007/978-3-319-15431-2.

Ritter, T., J. Euler, S. Ulbrich, and O. von Stryk (2016). Decentralized dynamic data-driven monitoring of atmospheric dispersion processes. *Procedia Computer Science 80*, 919–930. 10.1016/j.procs.2016.05.382.

Schneider, M., L. Halekotte, T. Comes, and F. Fiedrich (2026). Prioritisation recommendation mapping (prioremap): A method for supporting relief coordination in flood disaster response. *International Journal of Disaster Risk Reduction 132*, 105949. 10.1016/j.ijdrr.2025.105949.

Schneider, M., L. Halekotte, T. Comes, D. Lichte, and F. Fiedrich (2025). Emergency response inference mapping (erimap): a bayesian network-based method for dynamic observation processing. *Reliability Engineering & System Safety 255*, 110640. 10.1016/j.ress.2024.110640.

Schwerdtner, P. and B. Peherstorfer (2024). Greedy construction of quadratic manifolds for nonlinear dimensionality reduction and nonlinear model reduction. 10.48550/arXiv.2403.06732.

Snoun, H., M. Krichen, and H. Chérif (2023). A comprehensive review of gaussian atmospheric dispersion models: current usage and future perspectives. *Euro-Mediterranean Journal for Environmental Integration 8*(1), 219–242. 10.1007/s41207-023-00354-6.

Veiga-Piñeiro, G., P. Dominguez, E. Aldao, G. Fontenla-Carrera, F. Veiga-López, E. B. Martin, and H. González-Jorge (2024). Physics-aware wind surrogate model for uav aerodynamic response assessment. *International Journal of Numerical Methods for Heat & Fluid Flow 35*(10), 3583–3604. 10.1108/HFF-11-2024-0857.

von Danwitz, M., I. Voulis, N. Hosters, and M. Behr (2023). Time–continuous and time–discontinuous space–time finite elements for advection–diffusion problems. *International Journal for Numerical Methods in Engineering 124*(14), 3117–3144. 10.1002/nme.7241.